American Journal of Chemical Engineering
2023; 11(6): 102-116
http://www.sciencepublishinggroup.com/j/ajche
doi: 10.11648/j.ajche.20231106.11
ISSN: 2330-8605 (Print); ISSN: 2330-8613 (Online)

Martynia annua and Balanite Endocarp Activated Carbons to Remove Hg^{2+} and Pb^{2+} in Prepared Solutions Using Fixed-Bed Adsorption Column

Abdulhalim Musa Abubakar[1, *], Yusufu Luka[1], John Sylvester Lebnebiso[1], Abuh David[1], Moses NyoTonglo Arowo[2]

[1]Department of Chemical Engineering, Faculty of Engineering, Modibbo Adama University (MAU), Yola, Nigeria
[2]Department of Chemical & Process Engineering, Moi University, Eldoret, Kenya

Email address:
abdulhalim@mau.edu.ng (Abdulhalim Musa Abubakar)

[*]Corresponding author

To cite this article:
Abdulhalim Musa Abubakar, Yusufu Luka, John Sylvester Lebnebiso, Abuh David, Moses NyoTonglo Arowo. (2023). *Martynia annua* and Balanite Endocarp Activated Carbons to Remove Hg^{2+} and Pb^{2+} in Prepared Solutions Using Fixed-Bed Adsorption Column. *American Journal of Chemical Engineering, 11*(6), 102-116. https://doi.org/10.11648/j.ajche.20231106.11

Received: October 26, 2023; **Accepted**: November 14, 2023; **Published**: December 26, 2023

Abstract: Mercury (Hg) and lead (Pb) exposures to humans are sometimes from water bodies, which may damage the liver, kidneys, reproductive and developmental systems, immune, nervous, cardiovascular systems and can pass from the lungs to the bloodstream thereby affecting the oxygen carrying ability of the blood. As a result, this research seeks to produce a distinct activated carbon (AC) from *Balanite aegyptiaca* fruit endocarp (BAE) and *Martynia annua* fruits (MAF) via 4 methodological steps including reagent preparation, feedstock impregnation, carbonization and chemical activation using KOH at 600℃, to adsorbed Pb and Hg ions (Pb^{2+} & Hg^{2+}) from an artificially prepared aqueous water solution. Proximate analysis, especially a fixed carbon and carbon yield contents of 97.68 and 87.62% for BAE and 94.94 and 91.97% for MAF initially reveals the potentials of the raw materials for AC production. Apart from 0.0017 equal porosity of ACs generated that portrays a low adsorption effect, surface areas of 1015.37 and 1080.15 m^2/g for BAE-AC and MAF-AC respectively, are high and within the standard range. Flow controllers to release the solution whose initial metallic ion concentration is 0.313 g/mL, was made to operate at 1.67, 4.2, 7.42, 9.86, 11.56 and 13.33 mL/s in a locally built 13cm bed height continuous fixed-bed column. Findings shows that breakthrough curves from Bohart-Adams model and the purely empirical Freundlich isotherm parameters collectively signals a great potential of BAE and MAF for the adsorption of Pb^{2+} and Hg^{2+}, making their ACs a viable resource for purifying contaminated water.

Keywords: Activated Carbon, *Balanite aegyptiaca*, *Martynia annua*, Breakthrough Curves, Adsorption Column

1. Introduction

Balanite aegyptiaca fruits (desert date) are obtainable in great quantities in the Sahel-zones of Africa (especially in the Sudan), but has become widely scattered all over the semi-arid zone of the continent, spreading from Jos to Yola, in some Northern part of Nigeria, as well as many Arab countries [1, 2]. Different parts of the plant, such as the ripe fruit, the mesocarp, kernel and the shell have their unique importance, including: as raw materials for the production of human food and feed for animals [3], potential for sugar fermentation and steroid manufacturing, activated carbon (AC) and charcoal production and protein and oil extraction. *Martynia annua* or Vichchida (in Gujarati), Bichu (Hindi), Devil's claw (English) and Kakanasika (in Sanskrit) on the other hand, are found in Mexico, Pakistan, Nigeria and India, on road sides, wastelands, and rubbish heaps [4, 5]. Their bark can be used to produce AC, while the fruit can serve as antidote to scorpion stings and local sedative [6]. Evidently, both fruits are real precursors for the production of AC. AC usage dates back to several millennia in the treatment of water, refining of beet sugar and corn syrup and presently to control gasoline emission from motor vehicles, separate steroids, vitamins and antibiotics from fermentation broth,

filter tar from cannabis smoke, remove contaminants from solutions during potassium hydroxide, soda ash and alum production, purify gas, alcohol and gold, extract metals, decolorize sugar and as air filters in gas masks and respirators. Due to their complex nature, they exist as polymer coated carbon, impregnated carbon, pellet, powdered, granular and extruded AC, with each having their specific application. During their use, it is vital to measure the methylene blue range, pore volume, abrasion number, total surface area (SA), apparent/bulk density, ash content, molasses number, particle size distribution, carbon density, iodine number, hardness, dichlorination half-value length, particle density abrasion resistance and adsorptive capacity of the type chosen for one purpose or the other [7, 8]. For example, the same authors mentioned that AC contains micropores, mesopores and macropores.

Adsorptive properties of AC are influenced by the presence of functional groups that renders its surface chemically reactive [9–11]. Specific capacity of a granular AC to adsorb heavy metals is connected to total SA available per unit weight of carbon [12], molecular surface attraction and the concentration of contaminants in the water stream. This capacity is affected by contact time, AC particle size, treatment capacity, shaking time and the carbon depth in the filter [13, 14]. Heavy metals (e.g., mercury, cadmium, lead and cobalt) are not biodegradable [15], and their presence in water bodies and land leads to them finding their way into living organisms, thereby causing diverse health implications in animals and humans (e.g., anemia and high blood pressures). It is hence necessary to device a means of getting rid of heavy metals from aqueous solutions. Normally, AC utilized for such purpose, can be obtained from sawdust, waste weed, charcoal, wood, bones, coal, nut shells, peat, paper, coconut shell, maize stems, sugarcane stems, flint stone, palm kernel shells etc. [6, 16, 17]. Best raw material for its manufacture must be low cost [9], sludge free, contain minimal organic material, must result in high quality activated product, long storage life and be readily available. Examined raw materials for the production of AC for utilization in the adsorption of one or more toxic waste substances, as shown in Table 1, reveals diverse range of factors affecting their performances.

Table 1. *AC Produced from Various Agricultural Materials Channeled into Adsorbent Usage.*

Feedstock Converted	Purpose	Correlation of Data	Effectiveness of the Feedstock	Source
Bamboo Granular AC	Elimination of organic contaminant from refinery wastewater	Freudnlich & Langmuir isotherms	Initial-final concentration = 378-152 mg/L and 58.7% removal efficiency	[18]
Peanut shell AC	Removal of pyridine from artificially contaminated aqueous solutions	Isotherm: Langmuir & Freundlich Kinetics: Lagergren	30-60 mg/L initial-final conc.; 45.94-36.458% removal of pyridine and; 5.513-8.75 mg/g adsorption capacity	[19]
Coconut shell AC	Removal of Mn(II) and Al(III) from drinking water	Langmuir isotherm	At 600℃ and pH = 8 (i) adsorption capacity of Al^{3+} = 0.957 mg/g & (ii) adsorption capacity of Mn^{2+} = 0.857 mg/g	[20]
Maize cob AC	Adsorption of heavy metals in paint industry effluent	Langmuir isotherm & Pseudo First Order kinetic models	Adsorption capacity = 4.866 mg/g; pore volume = 1.28 cm^3/g and; SA = 1195.12 m^2/g	[21]
Coconut shell AC	Removal of heavy metals from dye effluent	Langmuir isotherm	Adsorption capacity of (i) Pb = 24.4 mg/g, (ii) Hg = 17.24 mg/g & (iii) Cu = 10 mg/g	[22]
Unspecified AC	Adsorption of p-Nitrophenol for wastewater treatment	Langmuir, Double-Langmuir & Dubinin-Radushkevich	Adsorption capacity = 340, 350 & 365 mg/g. Slightly increase with decreasing particle size	[23]
Balanite AC & Martynia AC	Adsorption of lead and mercury from aqueous solution	Freundlich model	Adsorption capacity – Balanite AC: 7.128 mg/g (Pb^{2+}) & 6.436 mg/g (Hg^{2+}) and Martynia AC: 6.436 mg/g (Pb^{2+}) & 5.721 mg/g (Hg^{2+})	Present Study

Correlations of the adsorption results obtained with various isotherm models mentioned in Table 1, is evidently becoming more practiced in recent years. This study uniquely concentrates on the removal of heavy metals from prepared solution of mercury (Hg) and lead (Pb) solution in a fixed bed adsorption column. Explicitly, the work's objectives are to produce AC from BAE and MAF; construct a fixed bed adsorption column; test the effect of varying flowrates on the percent of metal ions adsorbed by the ACs; determine the adsorptive capacity of the AC produced from Bohart-Adams model and; use breakthrough curves to highlight the performances of the adsorbent applied at constant initial concentration. With reference to the objectives stated, similar studies exist in the literature, except for the used of BAE and MAF-AC. For instance, by varying the influent concentrations (i.e., 100, 200 & 300 mg/L) and the flowrates (i.e., 9, 13 and 18 mL/min) in an adsorption column, Nwabanne et al. [24] used rice husk AC to remove phenol and also studied the resultant adsorption breakthrough curves using 4 different models. Using similar models, maximum removal of Pb^{2+} by a chemically carbonized rubber wood sawdust was investigated in a continuous fixed-bed column by Biswas & Mishra [25]. Furthermore, in both batch and continuous process column study, Park et al. [26] tested similar model to establish the kinetics of the adsorption of nitrate ions on certain type of non-woven fabric. The entirety of the models in question are Belter, Chu1, Chu2, Bed Depth Service Time (BDST), Thomas, Yoon-Nelson, Clark, Wolborska, Empty Bed Residence Time (EBRT) and Bohart-Adams models [27–29].

2. Methodology

2.1. Equipment, Reagents and Glass Wares

As would be seen in the experimental steps followed to actualize the set objectives, materials shown in Table 2 were used in accordance to standard procedures described.

At the beginning, the glass wares were treated to remove all traces of dirt and chemicals that may affect the results of the experiment significantly. Detergent and tap water were used to wash the glass wares, before immersing in a 4M HNO_3 solution for 24 h. These were then washed with deionized water to remove traces of acidity. The glass wares were oven dried using Proctor and Schwartz oven drier at a constant temperature of 60°C. Pretreatment of glass wares shown in Table 2 were done each time they are used for a particular experiment to prevent contamination.

Table 2. *List of Laboratory Equipment and Reagents Used for the Experiment.*

Equipment	Reagents	Glass wares
1) Beakers 2) Filter Papers 3) UV Spectrometer-6705 4) VGP210 Atomic Absorption Spectrophotometer 5) 4824/2 Oven (5A, 200/50V 1200W 6) Desiccators 7) LF3 Muffle Furnace-(Max. temp. 1200ºC) 8) Crucible 9) HK-DC-320AS Electronic Weighing Balance 10) PHS-3E pH Meter 11) Mortar and pestle	1) Distilled water 2) Potassium hydroxide (KOH) 3) Phosphoric acid (H_3PO_4) 4) Hydrochloric acid (HCl) 5) 99% Lead nitrate [$Pb(NO_3)_2$] 6) 16M Nitric acid (HNO_3) 7) Tap water	1) 50 mL Beaker 2) 1000 mL Beaker 3) 1000 mL Volumetric flask 4) 250 mL Graduated cylinder 5) 7 mm Stirring rod 6) 16×150mm Test tubes with screw caps

2.2. Agricultural Biomass Pretreatment

Balanite fruit was obtained from the market and the epicarp removed to free the seed. What follows was the soaking of the seed in water for 12 h to enable the mesocarp (soft flesh) to be washed away to free the endocarp. In contrast, *Martynia annua* was obtained along the road side within the premises of MAU, in North Eastern Nigeria. In this investigation, the endocarp shell and the *Martynia annua* seeds were the chief raw materials used. Both the endocarp shell and the *Martynia annua* seeds were washed with pipe born water [19, 30], sun dried and oven dried at 105oC for 1 h. Next, the Balanite seeds were crushed to free the endocarp shell from the kernel.

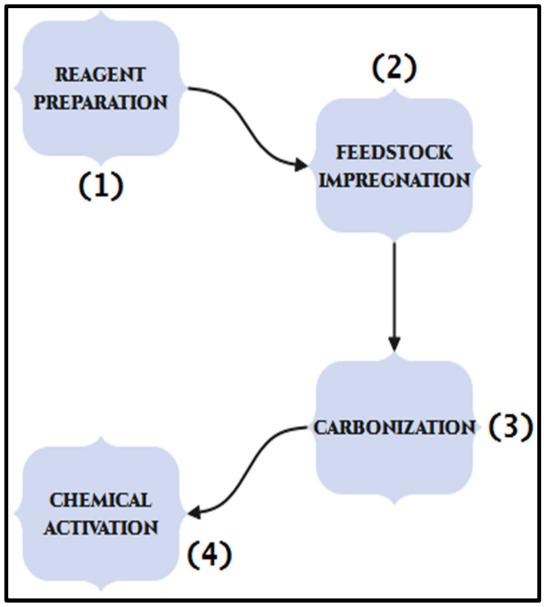

Figure 1. *Activated Carbon Production Flowchart.*

2.3. Activated Carbon Production Steps

A flowchart for AC production steps followed is shown in Figure 1.

Stage by stage experimental procedures based on literature report were designed to carry out each of the methodology mentioned.

2.3.1. Reagents Preparation

Volume of acids used to prepare standard solutions were calculated from Equation 1.

$$\text{Vol. Needed} = \frac{\text{Mola mass}(1000\text{ mL})(\text{Concentration Needed})}{1000(\%\text{ Purity})(\text{Specific Gravity})} \quad (1)$$

Water was first introduced into 1000 mL volumetric flask, followed by 1M H_3PO_4. In the next step, topping up of the flask to mark 1000 mL was carried out. This was done for the 3 different precursors used.

2.3.2. Doping of Feedstock

Feedstock (BAE, *Eucalyptus tereticornis* and MAF), each weighing 1000g were carefully introduced separately into a bowl containing 1M H_3PO_4 solutions, at the acid/precursor ratio of 2.5:1 (on weight basis). After which the content was stirred vigorously using a glass rod to give a homogeneous slurry mixture. The mixture was allowed to stand for 48 h. According to Okafor et al. [21], after this time interval, the feedstock is termed impregnated.

2.3.3. Carbonization

As the excess acid solution is removed by drying at 150℃, the process of converting the precursor to carbon was carried out. About 1000g of the impregnated feedstock mixture was then transferred into a muffle furnace bit by bit in crucibles. For 60 min and at temperature between 450-545℃ for BAE, 401-430 ℃ for MAF and 420-456 ℃ for *Eucalyptus tereticornis*, the samples were lastly carbonized. Now, the

charred produce was allowed to cool to room temperature before grounding to workable particle size, as also reported by Ademiluyi et al. [18]. The sample was then washed with tap water to a pH of 6.67 and dried in an oven at 125℃ for 60 min, similar to the methodology followed by Shendkar et al. [6]. Last of all, the percentage yield of the carbonized product was determined from the difference in the weight of the raw sample and the carbonized sample that was obtained.

2.3.4. Chemical Activation

Chemical activation was carried out in a muffle furnace using KOH as activating reagents, in accordance with Stephen et al. [31]. Around 1000g sample of the purified carbon was mixed with 1500 mL of 1M KOH stirred and heated until paste formation. It was placed in a muffle furnace at 600℃ for 1 h, allowed to cool to room temperature, washed with distilled water until a pH of 6.80 was read, dried at 100℃ in oven for 30 minutes and packed in an airtight container – making it ready for use.

2.4. Prospective Adsorbents Proximate Analysis

2.4.1. Moisture and Volatile Content

To be precise, 10g of sample was weighed and placed in the oven at 105°C for 30 min. It was then removed, cooled in a desiccator and re-weighed. Using Equation 2 [32], the percentage moisture content (MC) of the sample was determined. Same sample weight of the AC was weighed into a clean pre-weighed crucible and placed in the furnace at a temperature of 450℃ for 10 min. The sample was retrieved and left to cool in a desiccator. Afterwards, the weight of the sample before and after heating was used to determine the amount of volatile matter (VC) present in the sample by Equation 3 [7].

$$\text{Moisture content (\%)} = \left(\frac{W_i - W_f}{W_i}\right) \times 100 \quad (2)$$

$$\text{Volatile Content (\%)} = \left(\frac{W_0 - W_1}{W_0}\right) \times 100 \quad (3)$$

Where, W_i and W_f are weight of sample before and after drying and W_0 and W_1 are weights of the sample before and after heating. Normally, larger weight loss of the substance implies greater volatile matter content.

2.4.2. Ash Content

BAE sample (10g) were placed into a porcelain crucible and transferred into a muffle furnace set at a temperature of 900°C. The furnace was left ON for 1 hour, after which the crucible and content was transferred into a desiccator and allowed to cool. Subsequently, crucible and content were reweighed and the weight noted. Precent ash (PA) was then calculated using Equation 4 [33], where, W_0 = dry weight of the sample (g) and W_{ash} = constant weight after drying.

$$\text{Ash Content (\%)} = \frac{W_{ash}}{W_0} \times 100 \quad (4)$$

2.4.3. Carbon Yield and Fixed Carbon Content

Carbon yield (CY) from the dried weight, W_0 of the carbon sample (g) was determined by Equation 5 given by Kwaghger & Ibrahim [33]. On the other hand, the fixed carbon content (FC) was determined by subtracting the PA, MC and VC from CY, and again dividing by CY, as founded in Okafor et al. [21] and given by Equation 6.

$$\text{CY} = 100\left(\frac{W_{fC}}{W_0}\right) \quad (5)$$

$$\text{FC} = \left(\frac{\text{CY} - \text{MC} - \text{VC} - \text{PA}}{\text{CY}}\right) \times 100 \quad (6)$$

CY and FC are both percentage measurements, where, W_{fC} is the weight of carbon retrieved from furnace (g).

2.4.4. Burn-off

Getting the percent burn involves measuring 10g of sample into a clean pre-weighed crucible, before placing them in a furnace at 450℃ for 20 min. After this step, the mass of the sample was measured after carbonization to obtain the weight loss on carbonization using Equation 7.

$$\%\ \text{Burn} = \frac{W_{BC} - W_{AC}}{W_{BC}} \times 100 \quad (7)$$

By definition, W_{BC} and W_{AC} are weights of sample before and after carbonization [34, 35].

2.4.5. pH Measurement

A pH electrode was inserted into the washed samples and the pH value read from the meter. Samples with undesirable pH values were re-washed until a pH value between 6.80 was obtained.

2.5. Characterization of the AC Produced

2.5.1. Pore Volume, Bulk Density and Porosity

AC weighing 10g was soaked in 10 mL distilled water and boiled for 20 min to displace the air contained in the pores. The sample was filtered, left to dry and the final weight obtained was used to calculate the pore volume (PV), applying Equation 8. As for the bulk density (BD), a known volume of beaker was weighed and tightly packed with AC. The weight of the beaker with the sample was measured and the BD computed by Equation 9. Lastly, by simply multiplying BD with PV, the porosity was calculated based on Equation 10.

$$\text{Pore Volume} = \frac{W_i - W_f}{\text{Density of Water}} \quad (8)$$

$$\text{Bulk Density} = \frac{\text{Mass of AC}}{\text{Volume Occupied}} \quad (9)$$

$$\text{Porosity} = \text{Bulk Density} \times \text{Pore Volume} \quad (10)$$

Where, W_f and W_i are final and initial weights of the AC. Equations 8-10 were accessed from the literature [21, 33].

2.5.2. Surface Area Determination

Here, the specific SA of the AC was determined using standard solution of methylene blue (MB) prepared by dissolving 3.2g of MB in 1000 mL of distilled water to produce 0.0032M concentration of the MB. About 7g of the AC was introduced into the standard solution and allowed for

12 h, after which the AC was filtered from the solution and the concentration was determined using UV spectrometer [36] by serial dilution technique. Absorbance was plotted against concentration. The difference between the initial and the final concentration of the equilibrium solutions was noted and the number of molecules which is the amount of MB adsorbed onto the monolayer of the AC was calculated. Results obtained was then used to calculate the SA.

2.6. Preparation and Digestion of Effluent Sample

A standard solution of 0.3104M of Hg and Pb were prepared. Two mL of the effluent was weighed and introduced into 50 mL beakers. Around 20 mL of the digestion mixture (hypochloric acid and nitric acid) was introduced into the beakers. The sample was digested for 1 h at 175℃ and then filtered into 100 mL standard volumetric flask with the Whatman No.1 qualitative circles, 110 mm filter paper. After that, the filtrate was made up to the mark with distilled water and labeled accordingly.

Figure 2. *Designed Column Experimental Setup.*

2.7. Analysis and Testing

Concentrations of the feed and samples were determined using the Flame Atomic Absorption Spectroscopy (FAAS); specifically, the Atomic Absorption Spectrophotometer-VGP210. Hence, the concentrations of the samples were determined using a calibration curve generated during the calibration of the instrument.

2.8. Design and Fabrication of Column

A column was designed and fabricated to be able to perform down-flow continuous fixed-bed adsorption. The column is made of plastic pipe with a height of 97.7 cm and an inner diameter (d) of 2.4 cm. Attached to the original components of the apparatus was the column. This apparatus is composed of a solution supply basin and a beaker to collect the treated water [37]. Figure 2 depicts the fabricated column.

AC was placed between two perforated plastics attached to a plastic rope and then loaded into the column shown in Figure 2. This plastic rope is to enable easy loading and unloading of AC into and from the column. These plastics held the AC as a fixed-bed. Thus, the plastic rope and the perforated plastics are movable so that height of the bed could be adjusted depending on the length of the bed and the calculated entry length. It was actualized for the reason that, longer bed holds more adsorbent, allowing longer online time before regeneration is needed, in order to get a realistic pressure drop, breakthrough time and cost, as stated by Gabelman [38].

2.8.1. Adsorption Column Setup

Fixed bed column studies were carried out using a glass column of 97.7 cm internal diameter and 2.4 cm length. An AC having 1.5 mm particle size range was used. It is later packed into the column with a layer of plastic disc and filter paper at the bottom, as shown in Figure 2. Bed height of 13 cm was used for both AC produced. The tank containing the heavy metal solution was placed at a higher elevation so that the metal solution could be introduced into the column by gravitational flow. Tank A delivers the solution to Tank B at a constant flow rate. Tank B is equipped with a tap to help maintain a constant solution level in Tank A in order to avoid fluctuation of the flow rate of the solution being delivered to the column. Flow controllers are the tap in both tanks; to help regulate the flow rates. Six flow rates (1.67, 4.20, 7.42, 9.86, 11.56 and 13.33 mL/s) were used. The effluent samples were collected at specified intervals and analyzed for the residual concentrations of Hg^{2+} and Pb^{2+} using AAS at 217 nm, similar to guidelines in Kumar & Acharya [39]. Using Equation 11 [40], the percentage metal adsorbed by the respective ions was calculated and tabulated.

$$\% \text{ Adsorbed} = \frac{C_0 - C}{C_0} \times 100 \tag{11}$$

Where, C = concentration at any time, t (g/mL) and C_0 = initial Pb^{2+} or Hg^{2+} concentration (0.31 g/mL). In this study, C_0 of the metals present in the aqueous solutions are same.

2.8.2. Performance of AC Adsorption Column

In order to predict the performance of a continuous flow AC filter, a relationship based on a surface reaction rate theory can be employed. Consequently, Bohart–Adams or Logit method in form of Equation 12-14 [24, 39] were collectively used to evaluate the performance of an AC filter having a continuous flow pattern.

$$\ln\left[\frac{\frac{C}{C_0}}{1-\frac{C}{C_0}}\right] = -\frac{K_{ba}N_0X}{V} + K_{ba}C_0t \tag{12}$$

$$\ln\left[\frac{C}{C_0 - C}\right] = -\frac{K_{ba}N_0X}{V} + K_{ba}C_0t \tag{13}$$

$$t = \frac{V_E}{Q_w} \quad (14)$$

Where, K_{ba} = adsorption rate constant (mL/g-s), N_0 = adsorption capacity constant (g/mL), X = bed depth (13 cm), V = approach velocity or linear flowrate (cm/s), t = time required to completely exhaust the bed or the time required for the exchange zone to become established and move completely out of the bed (s), V_E = cumulative volume of wastewater passed through the bed or volume of wastewater treated to the point of exhaustion (200 mL) and Q_w = wastewater flowrate (mL/s). Using the cross-sectional area of the pipe, $A = \frac{\pi d^2}{4}$, the expression, $Q_w = AV$ was used to determine V. Data collected during the laboratory tests would serve as the basis for the design of full-scale adsorption columns [13]. As would be carried out here, a successful design and operation of a fixed-bed column system require the production of the breakthrough curve for the effluent [23], which is simply a plot of C/C_0 against time.

2.8.3. Adsorption Isotherm

Freundlich model given by Equation 15 [41] was used through nonlinear curve fitting in ORIGIN Pro to determine their unknown parameters.

$$q_e = KC_e{}^{1/n} \quad (15)$$

By definition, $K =$ constant related to the adsorption capacity (μg/g mL), $n =$ empirical constant related to the intensity of adsorption (dimensionless), q_e = amount of the solute adsorbed per unit mass of the adsorbent (mg/g), also calculated using Equation 16 [40], C_e = final/equilibrium concentration (or C), M = mass of adsorbent used, $V_{ad} = V_E =$ volume of contaminated water used (mL) and C_i = initial concentration (or C_0) (in g/mL).

$$q_e = \frac{(C_i - C_e)V}{M} \quad (16)$$

Having obtained q_e and C_e set of values from empirical results computations utilizing relevant equations and analytical equipment, Equation 15 was specified as a user-defined non-linear model in Origin software to give K and n values, based on q_e vs. C_e fitted plots.

3. Results and Discussion

3.1. Upshot of Proximate Analysis of Samples

Proximate analysis result of BAE and MAF fruits are shown in Table 3.

Table 3. *Proximate Analysis for the Two Potential Adsorbents.*

Analysis	Composition (%)	
	Balanite aegyptiaca **Fruit Endocarp**	***Martynia annua*** **Fruits**
Ash Content	2.32	5.05
Moisture Content	0.02	0.03
Volatile Content	81.96	93.92
Fixed Carbon	97.68	94.94
Burn Off	12.38	8.03
Carbon Yield	87.62	91.97

MC in the seeds of Balanite fruits reported previously are 5.2% and 4.56%, which are more than the amount found in their endocarp, based on empirical results of Murthy et al. [1] and Wakawa et al. [32] respectively. Though expected, hardly any study reports the MC of its endocarp which is 0.02% in this study. Saka et al. [42] confirms that the carbon content in all peels renders them viable for AC production. Therefore, an FC of 97.68 and 94.94% for the respective BAE and MAF, makes them a good AC precursor, which also conforms with literature reports of Kwaghger & Ibrahim [33]. A higher burn-off percent or burn-off yield > 12.38 and 8.03% shown in Table 3, would be preferable for a material use to produce AC – typically between 40-60% for majority of other applications according to the literature. Chang et al. [43] previously obtained 59 and 71wt% burn-off of steam and carbon dioxide activations, respectively, indicating high adsorptive capacity as against this study having very low burn-off yield that is by far outside the desired range. There is however a complex relationship between burn-off and the microporous material for AC formation, as stated by Kwiatkowski & Kopac [44]. But 87.62% and 91.97% CY is relatively high, and surely a good property in the manufacture of AC. Proximate data in Table 3 are breakthrough analysis assay for both BAE and MAF; given that almost all previously related researched works are void of these results.

3.2. Outcome of AC Characterization

Clearly observed in Table 4 was that, as the temperature of carbonization increased from 400–550℃, the PVs of the AC is 0.0023 mL/g and 0.0032 mL/g respectively for the samples, at 1M H_3PO_4. These values are within the range of 0.68–2.8 cm^3/g reported by Kwaghger & Ibrahim [33] for mango nuts and 0.095 cm^3/g for *Parkia speciosa* by Foo & Lee [30]. By comparison, mango nuts will have the greatest capacity for adsorbing heavy metals, since it has the largest PV, followed by *Parkia speciosa*, MAF and BAE.

Concentration of H_3PO_4 and KOH chloride solutions with temperature, are critical parameters that control the final pore in the carbon. However, activation with KOH at 650℃ gave the best results with PV of 2.3 cm^3/g, as exemplified in Okafor et al. [21]. Primary reason for this occurrence is that the higher concentration leads to a better phosphorylation of the lignin and cellulose molecules present in the precursors. Temperature higher than 500 ℃ causes the cross linkages between the phosphate esters which make them unstable, leading to a drop in PV. AC produced based on this temperature gave BD values ranging from 0.74–0.54 g/mL, as shown in Table 4.

Table 4. *Characterized AC Produced at 400-500*℃.

Parameters	AC Source	
	Balanite aegyptiaca **Fruit Endocarp**	***Martynia annua*** **Fruits**
Bulk Density (g/mL)	0.74	0.54
Pore Volume (mL/g)	0.0023	0.0032
Porosity	0.0017	0.0017
Surface Area (m^2/g)	1015.37	1080.15
Particle Size (mm)	1.50	1.50

This BD at 500℃, conforms with the standard range (i. e., 0.3–0.4 g/mL). Therefore, carbonization at 500℃ with 1M H_3PO_4 and KOH gave optimum results that would produce suitable capacity for adsorption. By extension, an increase in porosity in accordance with Okafor et al. [21] corresponding to similar increase in concentration of activating acid, was the result of matrix expansion in the structure of the carbon. However, a deviation from the standard value (0.42-2.2) could be the resultant effect of parameters such as soaking time and rate of heating, that were hitherto, not studied. Porosity is a function of PV [45]. Typical PVs ranges from 0.5-1.0 mL/g (cm^3/g). In this case, a PV of 0.0023 and 0.0032 mL/g would have limited adsorption capacity of heavy metals. SAs of 1015.37 m^2/g and 1080.15 m^2/g were achieved at 500℃ with 1M H_3PO_4 and KOH ratio of 1:1 for both BAE and MAF, respectively. An increase in temperature will cause reduction in SA. Upon treatment with KOH, the SA as well as the PV increased. Literature standard range of 500-1500 m^2/g is in agreement with the SAs in this study. If compared with 336.35 m^2/g SA of rice husk AC [12] and 190 m^2/g SA of *Parkia speciosa* [30], it can be concluded that the biomass used for AC production in this study will have better adsorption capacity due to their higher SAs. Also note that the size of the AC particle has an opposite impact on the pressure drop across the bed and the intraparticle diffusion resistance and hence on the overall adsorption process.

3.3. Methylene Blue Absorbance by AC

Earlier, to determine the SA of the AC produced, the Brunauer-Emmett-Teller (BET) equation was used to determine the absorbed MB by the AC produced. A standard of 5 different mass concentrations were prepared and from a plot of absorbance against concentration done (Figure 3), the fraction adsorbed by the various AC were determined and presented in Table 5.

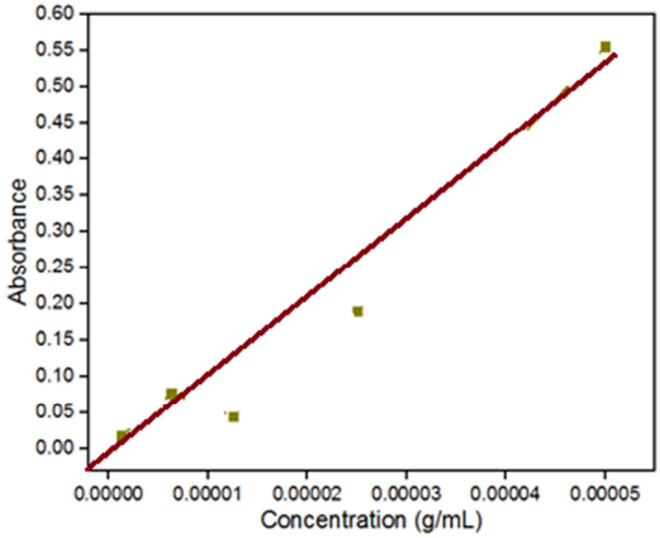

Figure 3. *Calibration Curve for Methylene Blue.*

Table 5. *MB Absorbance by the AC Produced.*

Precursor	Initial Conc. (g/mL)	Final Conc. (g/mL)	% Absorbed
Balanite AC	3.2×10^{-3}	2.05×10^{-6}	99.9
Martynia AC	3.2×10^{-3}	2.12×10^{-6}	99.9
Commercial AC	3.2×10^{-3}	2.01×10^{-6}	99.9

A calibration curve or plot of absorbance against concentration for MB typically follows Beer-Lambert law [46], which states that absorbance (A) is directly proportional to concentration of the analyte. Unlike stated, the concentration of MB doesn't increase linearly as 'A' increases. Adjustments made is to draw a straight dark red line that passes through the origin (0, 0). Normally, the function of the curve in Figure 3 is to quantitively determine the concentration of MB in unknown samples by measuring their absorbance and then using the linear relationship derived from the curve to calculate the concentrations arrived at in Table 5 [47]. Potential reasons for the existence of a non-linear relationship in Figure 3 might be due to non-linear absorption behavior, chemical reactions and/or instrument limitations. Nevertheless, it appears that all 3 types of ACs (BAE, MAF and commercial) have similar final concentrations of MB absorbance, with values very close to each other: 2.05×10^{-6}, 2.12×10^{-6} and 2.01×10^{-6} g/mL. It means that, under the specified conditions and at the equal initial concentration of 0.0032 g/mL, the 3 types of AC have similar adsorption capabilities for MB. The very close final concentrations suggest that they are all effective at adsorbing MB from the solution, and there is no significant difference in their adsorption performance based on the provided data.

3.4. Valuation of Adsorption Column Design Parameters

3.4.1. General Findings and Computations

About 8.39 g of the AC produced (or M) were used in the 13 cm bed height. As already defined in the methodology and as obtained in this study, percentage of each heavy metal

adsorbed was calculated as well as the C/ C_0 values to facilitate the reproduction of the breakthrough curves using Balanite and Martynia AC, as demonstrated in Tables 6-8.

Table 6. *Amount of Lead and Mercury Removed by Balanite AC at Different Flowrates.*

Q_w (mL/s)	C_0 (g/mL)	Pb^{2+} Removed			Hg^{2+} Removed		
		C (g/mL)	% Adsorbed	C/C_0	C (g/mL)	% Adsorbed	C/C_0
1.67	0.31	0.011	96.452	0.035	0.04	87.097	0.129
4.20	0.31	0.02	93.548	0.065	0.07	77.419	0.226
7.42	0.31	0.05	83.871	0.161	0.11	64.516	0.355
9.86	0.31	0.1	67.742	0.323	0.14	54.839	0.452
11.56	0.31	0.14	54.839	0.452	0.17	45.161	0.548
13.33	0.31	0.16	48.387	0.516	0.21	32.258	0.677

Table 7. *Amount of Lead and Mercury Removed by Martynia AC at Different Flowrates.*

Q_w (mL/s)	C_0 (g/mL)	Pb^{2+} Removed			Hg^{2+} Removed		
		C (g/mL)	% Adsorbed	C/C_0	C (g/mL)	% Adsorbed	C/C_0
1.67	0.31	0.04	87.097	0.129	0.07	77.419	0.226
4.20	0.31	0.09	70.968	0.290	0.10	67.742	0.323
7.42	0.31	0.13	58.065	0.419	0.13	58.065	0.419
9.86	0.31	0.16	48.387	0.516	0.16	48.387	0.516
11.56	0.31	0.185	40.323	0.597	0.185	40.323	0.597
13.33	0.31	0.21	32.258	0.677	0.21	32.258	0.677

Table 8. *Amount of Lead and Mercury Removed by Commercial AC at Different Flowrates.*

Q_w (mL/s)	C_0 (g/mL)	Pb^{2+} Removed			Hg^{2+} Removed		
		C (g/mL)	% Adsorbed	C/C_0	C (g/mL)	% Adsorbed	C/C_0
1.67	0.31	0.01	96.774	0.032	0.03	77.419	0.097
4.20	0.31	0.06	80.645	0.194	0.08	67.742	0.258
7.42	0.31	0.11	64.516	0.355	0.14	58.065	0.452
9.86	0.31	0.13	58.065	0.419	0.17	48.387	0.548
11.56	0.31	0.19	38.710	0.613	0.21	40.323	0.677
13.33	0.31	0.21	32.258	0.677	0.26	32.258	0.839

What is referred to as the breakthrough curve is simply a plot of C/C_0 against time. Equation 14 gives the time needed for the exchange zone to become established and pass wholly out of the bed, as shown in Table 9. It was evaluated by taking specified Q_w values and final velocity, V = 2.946 cm/s.

Table 9. *Auxiliary Data to Plot the Breakthrough Curves and the Linearized Logit Model.*

	Balanite AC		Martynia AC		Commercial AC		
	$C_0 - C$	$\ln\left[\frac{C}{C_0-C}\right]$	$C_0 - C$	$\ln\left[\frac{C}{C_0-C}\right]$	$C_0 - C$	$\ln\left[\frac{C}{C_0-C}\right]$	t (s)
Pb^{2+}							
	0.299	-3.3025483	0.27	-1.90954	0.3	-3.4012	119.7605
	0.29	-2.67414865	0.22	-0.89382	0.25	-1.42712	47.61905
	0.26	-1.64865863	0.18	-0.32542	0.2	-0.59784	26.95418
	0.21	-0.74193734	0.15	0.064539	0.18	-0.32542	20.28398
	0.17	-0.19415601	0.125	0.392042	0.12	0.459532	17.30104
	0.15	0.064538521	0.1	0.741937	0.1	0.741937	15.00375
Hg^{2+}							
	0.27	-1.9095425	0.24	-1.23214	0.28	-2.23359	119.7605
	0.24	-1.23214368	0.21	-0.74194	0.23	-1.05605	47.61905
	0.20	-0.597837	0.18	-0.32542	0.17	-0.19416	26.95418
	0.17	-0.19415601	0.15	0.064539	0.14	-0.194156	20.28398
	0.14	-0.19415601	0.125	0.392042	0.10	0.741937	17.30104
	0.10	0.741937345	0.1	0.741937	0.05	1.648659	15.00375

Note: Co–C is amount adsorbed in g/mL

Since commercial AC would mostly scale-through all standard test which was the basic reason for its commercialization, this study incorporates it to broaden the scope of the work. It is expected that subsequent analytical depictions of Balanite and Martynia AC for any of the ions, should tally with the trend or behavior displayed by the commercial result graphical lines. It will further test the extent of accuracy and precision in obtaining laboratory results for the selected AC performance.

3.4.2. Flowrate Influence

Pb and Hg ions adsorbed by the respective ACs from the 3 raw materials, regarded as the difference between their initial and final concentrations, can be related with the flowrates

studied. Back then, Gritti & Guiochon [47] looked at the effect of 3 different flowrates (0.5, 1 & 2 mL/min) on the amount adsorbed, where they both show proportional relationship. In this study (Figure 4), high adsorption occurs at low flowrates and as the flowrate rise, the amount of ions adsorbed by the raw materials ACs decline. More matched report was by Huang et al.[48], in which lower flowrate gives higher Pb (II) adsorptivity in a packed column.

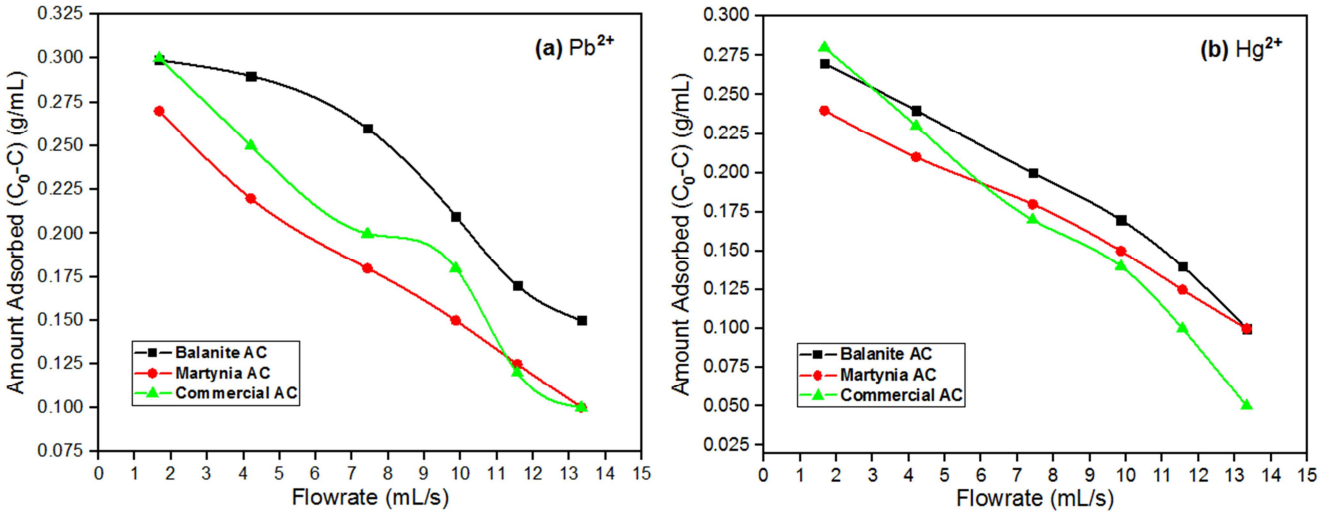

Figure 4. *Amount of (a) Pb^{+2} and (b) Hg^{2+} Adsorbed by Balanite, Martynia and Commercial AC at Different Flowrate.*

When Q_w = 1.67 mL/s, 96.5, 87.1 and 96.8% adsorption was obtained for Balanite, Martynia and commercial AC Pb^{2+} adsorption; while 87.1, 77.4 and 77.4% was obtained for Hg^{2+} adsorption. But, at the highest flowrate, Q_w = 13.33 mL/s, Pb^{2+} and Hg^{2+} adsorption rates were mostly < 33% (Tables 6-8). Knopp et al. [49] mentioned that insulin adsorption capacity decreased hyperbolically with flowrate for both polyethylene and polyvinyl chloride. In addition, at flowrates of 9, 13 and 18 mL//min, Nwabanne et al. [24] discovered that the adsorption capacity of rice husk AC decreased with an increase in the flowrate of the phenol solution in a parked column. Obviously, sufficient study derived from previous literature works, satisfy the pattern of changes of the flowrates with the amounts of ions adsorbed by the ACs used in this study.

3.4.3. Bohart-Adams Model Constants

K_{ba} and N_0 values can be harvested from linearized plots of $\ln\left(\frac{C}{C_0-C}\right)$ vs. t shown in Figures 5-7, calculated from slope = $K_{ba}C_0$ and intercepts = $-K_{ba}N_0X/V$ of the straight line produced. Insufficient fitting of the points was exhibited by all the plots in the graphs. For Pb^{2+} adsorption, commercial AC is ranked highest based on coefficient of determination (R^2) obtained followed by Martynia, then Balanite AC. Still, commercial AC comes first based on R^2 value gotten, followed by Balanite and Martynia AC for Hg^{2+} adsorption from the aqueous solution. But the AC whose R^2 value is closest to the commercial estimate or even surpasses it (approaching unity), will serve as the best performing precursor. The best AC precursor for both metal ions are ranked as follows: Commercial, Martynia and Balanite.

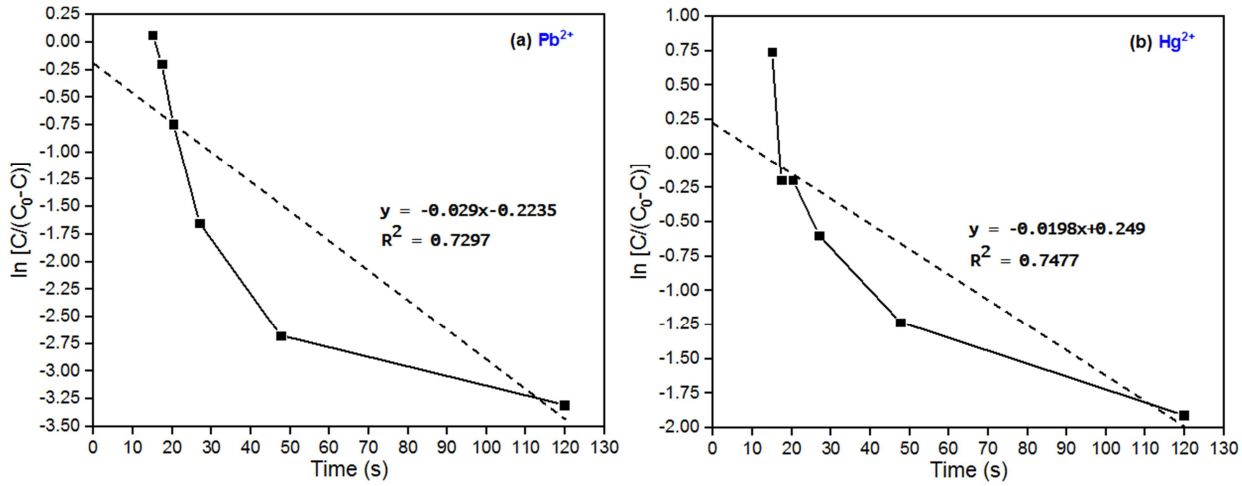

Figure 5. *Linearized Form of Logit Model for Balanite AC.*

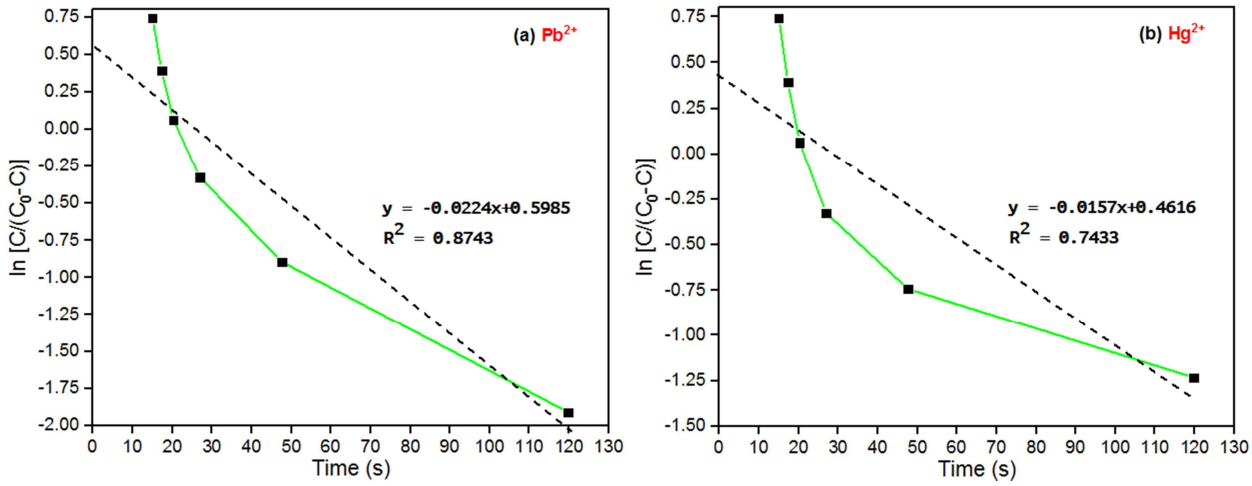

Figure 6. *Linearized Form of Logit Model for Martynia AC.*

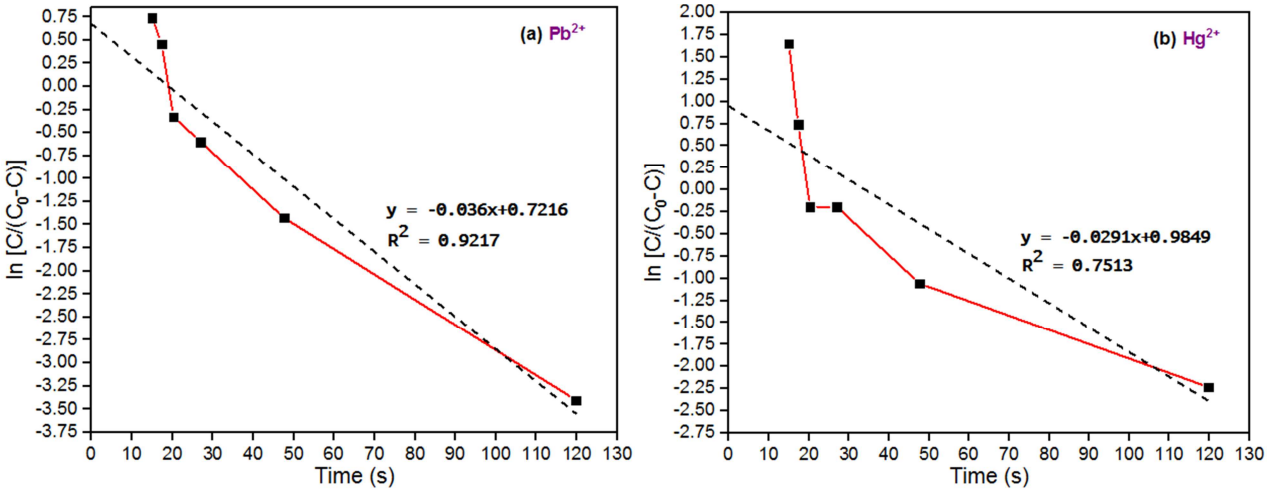

Figure 7. *Linearized Form of Logit Model for Commercial AC.*

Values of K_{ba} and N_0 obtained (Table 10) were –0.0935 & –0.0723 mL/g.s and –0.5414 & 1.8770 g/mL for BAE and MAF-AC, respectively for the adsorption of Pb^{2+}. For Hg^{2+} adsorption using BAE and MAF-AC, the same parameters are –0.0639 & –0.0506 mL/g.s and 0.8835 & 2.0655 g/mL, respectively. As stated by Kumar & Acharya [39], these parameter values may well be used for the design of adsorption columns. Regrettably, negative K_{ba} can be indicative of errors in the experimental data, such as inconsistencies, outliers, or measurement inaccuracies.

Table 10. *Adsorption Rate & Adsorption Capacity Constants Computed from the Linear Equations of Figures 5-7.*

AC Precursor	**Heavy Metal**			
	Pb^{2+}		**Hg^{2+}**	
	K (mL/g-s)	**N_0 (g/mL)**	**K (mL/g-s)**	**N_0 (g/mL)**
Balanite endocarp	−0.093548	−0.54142	−0.063871	0.883457
Martynia annua	−0.072258	1.877013	−0.050645	2.065462
Commercial	−0.116129	1.408138	−0.093871	2.377663

Bohart-Adams model is normally based on certain assumptions about the adsorption process. As such, deductions from this study points to non-conformity of the experimental system with the model assumptions, and hence the negative K_{ba}-s. It may also suggest that desorption was dominant over adsorption. However, on whether the model of choice is the problem, different adsorption conditions must be tested before making such conclusion. Again N_0 cannot be negative. In the case of BAE AC (where, N_0 = –0.5414 g/mL), it is either the experimental data for Pb^{2+} is unreliable or the Bohart-Adams model is not suitable for describing Pb^{2+} adsorption under the given conditions. Positive N_0 (0.8835 g/mL) for Hg^{2+} makes more sense and satisfy the model assumption. Overall, a combination of K_{ba}-negative and N_0-positive situation for a particular metal ion is still unsatisfactory.

3.4.4. Breakthrough Curves for Lead and Mercury Ions

In order to visualize how the concentration of the

adsorbate changes over time as it passes through the adsorption bed, breakthrough curves for the respective heavy metals were plotted, as showcased by Figures 8b and 9b. While flowrate can be important parameter in adsorption process, it is not typically used as x-axis in breakthrough curves. However, a comparison of the two types of curves: C/C_0 vs. Q_w [37] and C/C_0 vs. time (Gupta & Kumar, 2021) found in the literature, can be made. Decreasing C/C_0 as time increases, designates an effective removal of metal ions by the adsorbate from the influent stream of the system. Alternatively, C/C_0 surge with flowrate rise (Figures 8a and 8b) shows that the adsorption system is not keeping up with the higher flowrate. It implies that as the flowrate is increased, the adsorbent material is not able to capture the adsorbate as effectively, leading to higher concentrations of the adsorbate at the outlet.

Though, the shape of a breakthrough curve is not always S-shaped, typically realized when a bed of adsorbent material begins to adsorb the adsorbate until it reaches its adsorption capacity. In some cases, different curve shapes, such as sharp or steep breakthrough curves in systems with rapid adsorption (as in Figure 8a & 9a) or long tailing curves in situations where desorption is slow (as in Figure 8b & 9b), are encountered. Thus, the steep breakthrough curve of Figures 8-9 (a) are attributed to high adsorption capacity, slow flowrates, and high initial concentration (0.313 g/mL).

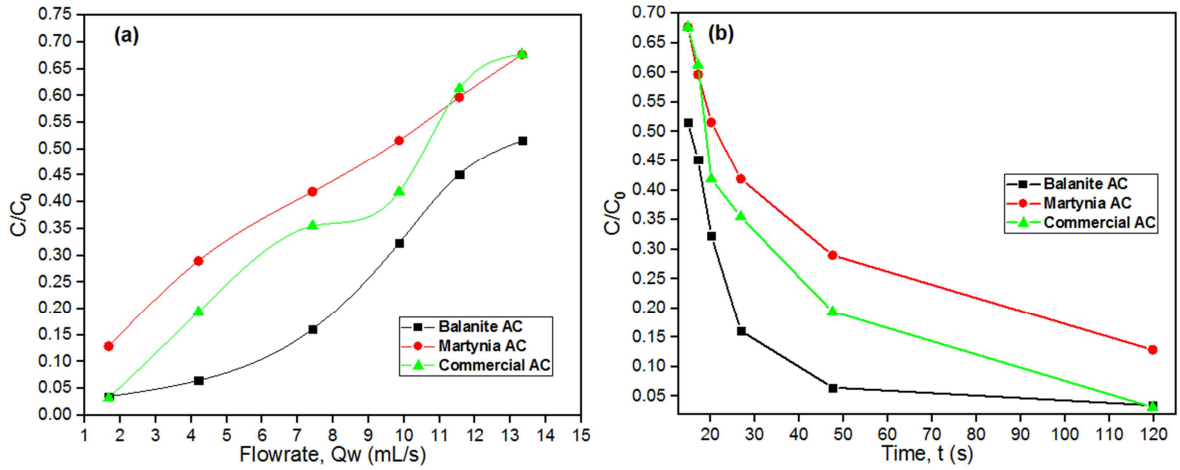

Figure 8. *Breakthrough Curve for Pb^{2+} in Terms of (a) Flowrate and (b) Time.*

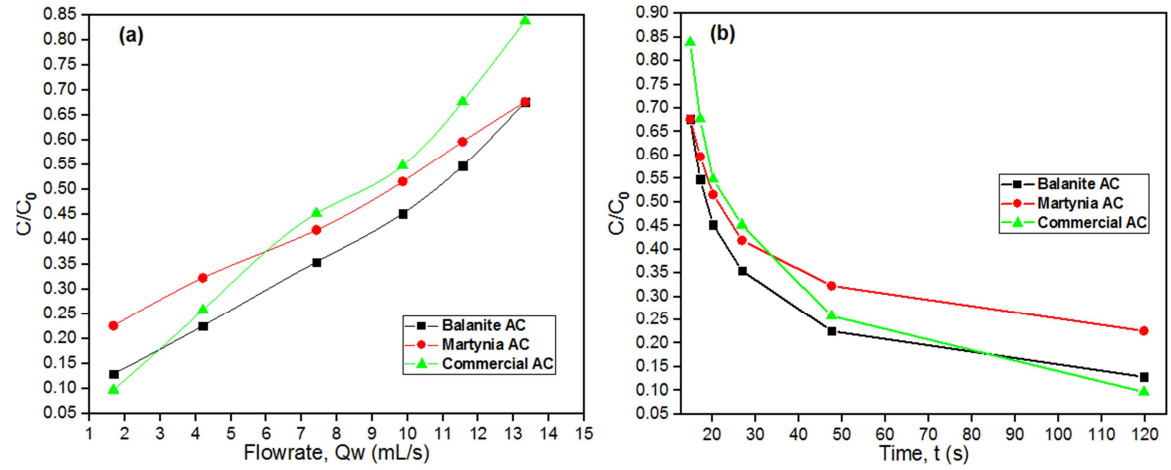

Figure 9. *Breakthrough Curve for Hg^{2+} in terms of (a) Flowrate and (b) Time.*

3.5. Implications of the Freundlich Constants Values

Even when the exact nature of the adsorbent is not known, Freundlich isotherm model provides good experimental fit, as in Figure 10, canceling the need for a detailed knowledge of the underlying adsorption mechanism. Freundlich model parameters comprising of 'K' related to the adsorption capacity and 'n' that gives information about the adsorption intensity, both offers insights into the adsorption process [51]. Preferably, the higher the 'K', the greater the adsorption capacity. For Balanite AC, the higher value of 'K' in Figure 10a for Pb^{2+} (i.e., 2.83436 μg/g mL) indicates that the AC is more effective at adsorbing Pb^{2+} from the aqueous solution compared to Hg^{2+}.

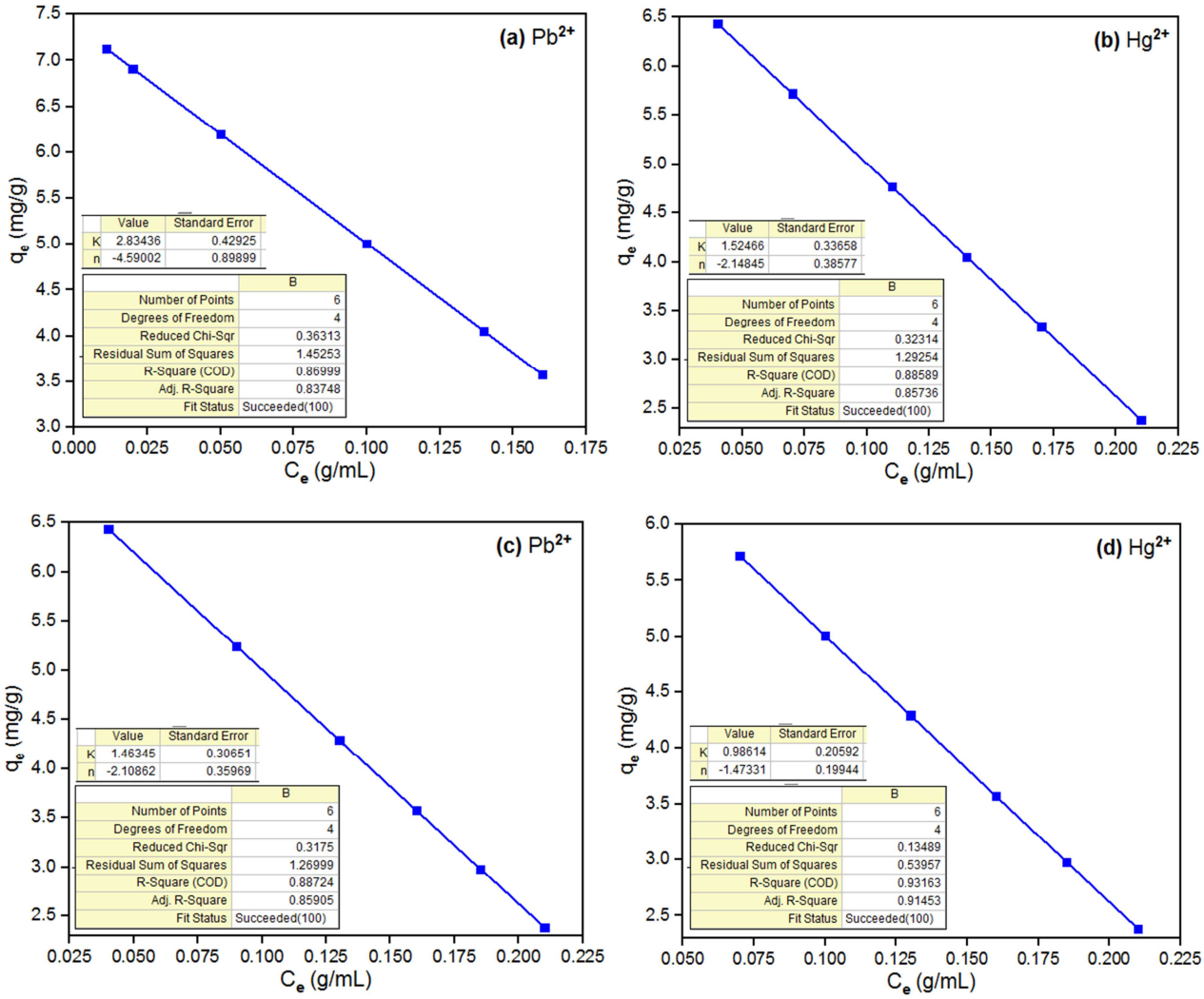

Figure 10. *Balanite AC (a) Pb^{2+} & (b) Hg^{2+} and Martynia AC (c) Pb^{2+} & (d) Hg^{2+} Isotherm Parameters from Freundlich Model.*

Similarly, the higher value of 'K' in Figure 10c for Pb^{2+} (i.e., 1.46345 μg/g mL) indicates that the Martynia AC is more effective at adsorbing Pb^{2+} from the aqueous solution compared to Hg^{2+} with lower K value = 0.98614 μg/g mL in Figure 10d. In general, adsorption by Balanite AC is greater than by Martynia AC, judging their performance using K-s harvested. Information about the shape of the adsorption isotherm can be reap from the 'n' values. If n ≅ 1, favorable adsorption process is exhibited (typical of monolayer adsorption) [52], n < 1 suggests cooperative or multilayer adsorption and n > 1 implies unfavorable adsorption. Results from this analytical study reveals the occurrence of a multilayer adsorption of both ions by the two adsorbents used. Hence, favorable adsorption occurred due to negative 'n' gotten in all, suggesting that the adsorption intensity decreases with increasing C_e (steep adsorption isotherm).

4. Conclusion

Effectiveness study of the use of BAE and MAF seed as natural resource for preparing AC and the progressive use of the resultant AC to adsorb Pb^{2+} and Hg^{2+} from aqueous solutions has been examined in this work. Sufficiently high FC (97.68% & 94.94%) and CY (87.62% & 91.97%) of the respective adsorbents makes them an AC precursor, while an SA of 1015.37 and 1080.15 m^2/g for Balanite and Martynia AC, respectively brands them as potentially good adsorbents, except for their low PVs which is a trade-off. When a total of 8.39 g of AC was employed to separately remove a prepared solution containing 0.313 mg/L Hg^{2+} and Pb^{2+} on a locally coupled fixed-bed column, it was found that maximum adsorption of the ions occurred at the lowest flowrate of 1.67 mL/s. But a probable adsorption challenge (e.g., low quality experimental findings, unsuitable model and measurement imprecision) is sensed owing to an entirely negative K_{ba}-s estimated from Bohart-Adams model for the adsorbents as well as the commercial AC performance, utilized as control and for comparability studies. All things considered, breakthrough curve realized, points to high adsorption capacity, low flowrates, and high initial concentration; while dependent vs. independent variable plots R^2 values, ranked the adsorbent effectiveness from Commercial, Martynia AC, then Balanite AC. Despite that, a negative K_{ba} from the Bohart-Adams model is a red flag that should prompt a

thorough examination of the experimental data, model assumptions and system conditions to determine the underlying reasons and potentially refine the approach to studying adsorption kinetics. Wolborska, Yoon-Nelson, Clark, Belter, Chu_1, Bed Depth Service Time (BDST) and Thomas linear column kinetic model equations are few other models the data in this study may be analyzed with. In addition, Balanite AC Pb^{2+} and Hg^{2+} adsorption performs better than Martynia AC, judging their performance using K-s realized from Freundlich isotherm model.

Conflicts of Interest

Authors declare no conflict of interest.

References

[1] H. N. Murthy, G. G. Yadav, Y. H. Dewir, and A. Ibrahim, "Phytochemicals and biological activity of desert date (Balanites aegyptiaca (L.) Delile)," *Plants*, vol. 10, no. 32, pp. 1–22, 2021, doi: 10.3390/plants10010032.

[2] A. J. Alhassan *et al.*, "Phytochemical screening and proximate analysis of Balanites aegyptiaca kernel," *Food Sci. Qual. Manag.*, vol. 74, pp. 37–41, 2018, [Online]. Available: www.iiste.org.

[3] N. A. Aviara, E. Mamman, and B. Umar, "Some physical properties of Balanites aegyptiaca nuts," *Biosyst. Eng.*, vol. 92, no. 3, pp. 325–334, 2005, doi: 10.1016/j.biosystemseng.2005.07.011.

[4] R. Kenwat, P. Prasad, T. Satapathy, and A. Roy, "Martynia annua: An overview," *UK J. Pharm. Biosci.*, vol. 1, no. 1, pp. 7–10, 2013, [Online]. Available: www.ukjpb.com.

[5] R. K. Gupta and R. B. Rathi, "Pharmacognostical and phytochemical screening of the root of Martynia annua linn," *J. Univ. Shanghai Sci. Technol.*, vol. 23, no. 1, pp. 299–311, 2021, doi: 10.51201/Jusst12568.

[6] C. D. Shendkar, R. C. Torane, K. S. Mundhe, S. M. Lavate, A. B. Pawar, and N. R. Deshpande, "Characterization and application of activated carbon prepared from waste weed," *Int. J. Pharm. Pharm. Sci.*, vol. 5, no. 2, pp. 527–529, 2013, [Online]. Available: https://innovareacademics.in/journal.ijpps/Vol5Issue2/6685.pdf.

[7] N. Samson and M. Louis, "Activated carbon from corn cob for treating dye waste water," *Environ. Sci. Indian J.*, vol. 10, no. 3, pp. 88–95, 2015, [Online]. Available: https://www.tsijournals.com/articles/activated-carbon-from-corn-cob-for-treating-dye-waste-water.pdf.

[8] B. Sivakumar, C. Kannan, and S. Karthikeyan, "Preparation and characterization of activated carbon prepared from Balsamodendron caudatum wood waste through various activation processes," *RASAYAN J. Chem.*, vol. 5, no. 3, pp. 321–327, 2012, [Online]. Available: http://www.rasayanjournal.com.

[9] F. Chigondo, B. C. Nyamunda, S. C. Sithole, and L. Gwatidzo, "Removal of lead (II) and copper (II) ions from aqueous solution by baobab (Adononsia digitata) fruit shells biomass," *IOSR J. Appl. Chem.*, vol. 5, no. 1, pp. 43–50, 2013, [Online]. Available: www.iosrjournals.org.

[10] M. S. Shamsuddin, N. R. N. Yusoff, and M. A. Sulaiman, "Synthesis and characterization of activated carbon produced from kenaf core fiber using H3PO4 activation," in *5th International Conference on Recent Advances in Materials, Minerals and Environment (RAMM) & 2nd International Postgraduate Conference on Materials. Mineral and Polymer (MAMIP), 4-6 August 2015*, 2016, vol. 19, pp. 558–565, doi: 10.1016/j.proche.2016.03.053.

[11] A. R. Hidayu *et al.*, "Preparation of activated carbon from palm kernel shell by chemical activation and its application for β-carotene adsorption in crude palm oil," in *Journal of Physics Conference Series [ICoNSET 2019]*, 2019, vol. 1349, no. 012103, pp. 1–8, doi: 10.1088/1742-6596/1349/1/012103.

[12] A. Cheenmatchaya and S. Kungwankunakorn, "Preparation of activated carbon derived from rice husk by simple carbonization and chemical activation for using as gasoline adsorbent," *Int. J. Environ. Sci. Dev.*, vol. 5, no. 2, pp. 171–175, 2014, doi: 10.7763/ijesd.2014.v5.472.

[13] N. Sazali, Z. Harun, and N. Sazali, "A review on batch and column adsorption of various adsorbent towards the removal of heavy metal," *J. Adv. Res. Fluid Mech. Therm. Sci.*, vol. 67, no. 2, pp. 66–88, 2020, [Online]. Available: www.akademiabaru.com/arfmts.html.

[14] K. K. Alau, C. E. Gimba, J. A. Kagbu, and B. Y. Nale, "Preparation of activated carbon from neem (Azadirachta indica) husk by chemical activation with H3PO4, KOH and ZnCl2," *Sch. Res. Libr.*, vol. 2, no. 5, pp. 451–455, 2010, [Online]. Available: www.scholarsresearchlibrary.com/archive.html.

[15] M. A. El Zayat, "Removal of heavy metals by using activated carbon produced from cotton stalks," AUC Knowledge Fountain, 2009.

[16] J. O. Okafor and P. E. Dim, "Preparation and characterization of activated carbon using palm kernel shells for industrial effluent purification," *Niger. J. Technol. Res.*, vol. 8, no. 1, 2013, doi: 10.4314/njtr.v8i1.88873.

[17] A. O. Dada, A. A. Inyinbor, and A. P. Oluyori, "Comparative adsorption of dyes unto activated carbon prepared from maize stems and sugar cane stems," *IOSR J. Appl. Chem.*, vol. 2, no. 3, pp. 38–43, 2012, doi: 10.9790/5736-0233843.

[18] F. T. Ademiluyi, S. A. Amadi, and N. J. Amakama, "Adsorption and treatment of organic contaminants using activated carbon from waste Nigerian bamboo," *J. Appl. Sci. Environ. Manag.*, vol. 13, no. 3, pp. 39–47, 2010, doi: 10.4314/jasem.v13i3.55351.

[19] M. Sadiq and S. Hussain, "An efficient activated carbon for the wastewater treatment, prepared from peanut shell," *Mod. Res. Catal.*, vol. 2, no. 4, pp. 1–9, 2013, doi: 10.4236/mrc.2013.24020.

[20] Z. Ghazali, R. Othaman, and P. Abdullah, "Preparation of activated carbon from coconut shell to remove aluminium and manganese in drinking water," *Adv. Nat. Appl. Sci.*, vol. 6, no. 8, pp. 1307–1312, 2012, [Online]. Available: http://www.aensiweb.com/old/anas/2012/1307-1312.pdf.

[21] J. O. Okafor, D. O. Agbajelola, S. Peter, M. Adamu, and G. T. David, "Studies on the adsorption of heavy metals in a paint industry effluent using activated maize cob," *J. Multidiscip. Eng. Sci. Technol.*, vol. 2, no. 2, pp. 39–46, 2015, [Online]. Available: www.jmest.org.

[22] L. I. Onyeji and A. A. Aboje, "Removal of heavy metals from dye effluent using activated carbon produced from coconut shell," *Int. J. Eng. Sci. Technol.*, vol. 3, no. 12, pp. 8238–8246, 2011, [Online]. Available: https://www.idc-online.com/technical_references/pdfs/chemical_engineering.

[23] B. Ledesma *et al.*, "Batch and continuous column adsorption of p-nitrophenol onto activated carbons with different particle sizes," *Processes*, vol. 11, no. 2045, pp. 1–22, 2023, doi: 10.3390/pr11072045.

[24] J. T. Nwabanne, O. C. Iheanacho, C. C. Obi, and C. E. Onu, "Linear and nonlinear kinetics analysis and adsorption characteristics of packed bed column for phenol removal using rice husk-activated carbon," *Appl. Water Sci.*, vol. 12, no. 91, pp. 1–16, 2022, doi: 10.1007/s13201-022-01635-1.

[25] S. Biswas and U. Mishra, "Continuous fixed-bed column study and adsorption modeling: Removal of lead ion from aqueous solution by charcoal originated from chemical carbonization of rubber wood sawdust," *J. Chem.*, vol. 2015, no. 907379, pp. 1–9, 2015, doi: 10.1155/2015/907379.

[26] H. J. Park, D. C. Nguyen, C.-K. Na, and C.-I. Kim, "Applications and limits of theoretical adsorption models for predicting the adsorption properties of adsorbents," *Water Sci. Technol.*, vol. 72, no. 8, pp. 1364–1374, 2015, doi: 10.2166/wst.2015.327.

[27] M. A. M. Altufaily, N. J. Al-Mansori, and A. F. M. Al-Qaraghulee, "Mathematical modeling of fixed-bed columns for the adsorption of methylene blue on to fired clay pot," *Int. J. ChemTech Res.*, vol. 12, no. 2, pp. 70–80, 2019, doi: 10.20902/IJCTR.2019.120210.

[28] K. N. Gupta and R. Kumar, "Fixed bed utilization for the isolation of xylene vapor: Kinetics and optimization using response surface methodology and artificial neural network," *Environ. Eng. Resour.*, vol. 26, no. 2, pp. 1–11, 2021, doi: 10.4491/eer.2020.105.

[29] L. C. Lau, N. M. Nor, K. T. Lee, and A. Mohamed, "Adsorption isotherm, kinetic, thermodynamic and breakthrough curve models of H2S removal using CeO2/NaOH/PSAC," *Int. J. Petrochemical Sci. Eng.*, vol. 1, no. 2, pp. 36–44, 2016, doi: 10.15406/ipcse.2016.01.00009.

[30] P. Y. L. Foo and L. Y. Lee, "Preparation of activated carbon from Parkia speciosa pod by chemical activation," in *Proceedings of the World Congress on Engineering and Computer Science 2010 Vol II [WCECS 2010, October 20-22, 2010, San Francisco, USA]*, 2010, pp. 696–698, [Online]. Available: https://www.iaeng.org/publication/WCECS2010/WCECS2010_pp696-698.pdf.

[31] A. E. Stephen, C. Gimba, A. Uzairu, and Y. A. Dallatu, "Preparation and characterization of activated carbon from palm kernel shell by chemical activation," *Res. J. Chem. Sci.*, vol. 3, no. 7, pp. 54–61, 2013, [Online]. Available: http://www.isca.me/rjcs/Archives/v3/i7/8.ISCA-RJCS-2013-095.pdf.

[32] A. I. Wakawa, A. B. Sambo, and S. Yusuf, "Phytochemistry and proximate composition of root, stem bark, leaf and fruit of desert date, Balanites aegyptiaca," *J. Phytopharm. (Pharmacognosy Phytomedicine Res.*, vol. 7, no. 6, pp. 464–470, 2018, [Online]. Available: www.phytopharmajournal.com.

[33] A. Kwaghger and J. S. Ibrahim, "Optimization of conditions for the preparation of activated carbon from mango nuts using HCl," *Am. J. Eng. Res.*, vol. 2, no. 7, pp. 74–85, 2013, [Online]. Available: www.ajer.org.

[34] H.-C. Hsi, R. S. Horng, T.-A. Pan, and S.-K. Lee, "Preparation of activated carbons from raw and biotreated agricultural residues for removal of volatile organic compounds," *J. Air Waste Manage. Assoc.*, vol. 61, no. 5, pp. 543–551, 2011, doi: 10.3155/1047-3289.61.5.543.

[35] H. Faltynowicz, J. Kaczmarczyk, and M. Kulazynski, "Preparation and characterization of activated carbons from biomass material-giant knotweed (Reynoutria sachalinensis)," *Open Chem*, vol. 13, pp. 1150–1156, 2015, doi: 10.1515/chem-2015-0128.

[36] S. Kananpanah, M. Ayazi, and H. Abolghasemi, "Breakthrough curve studies of purolite A-400 in an adsorption column," *Pet. Coal*, vol. 51, no. 3, pp. 189–192, 2009, [Online]. Available: www.vurup.sk/pc.

[37] M. Puspitasari, "Column performance in lead(II) removal from aqueous solutions by fixed-bed column of mango wood sawdust (Mangifera indica)," *J. Kim. Ris.*, vol. 3, no. 1, pp. 29–37, 2018, doi: 10.20473/jkr.v3.i1.7799.

[38] A. Gabelman, "Adsorption basics: Part 1," in *Back to Basics*, American Institute of Chemical Engineers (AIChE), 2017, pp. 48–53.

[39] U. Kumar and J. Acharya, "Fixed bed column study for the removal of copper from aquatic environment by NCRH," *Glob. J. Researccches Eng. Chem. Eng.*, vol. 12, no. 3, pp. 1–4, 2012, [Online]. Available: https://globaljournals.com.

[40] G. H. Haghdoost, H. Aghaie, and M. Monajjemi, "Investigation of Langmuir and Freundlich adsorption isotherm of Co2+ ion by micro powder of cedar leaf," *Orient. J. Chem.*, vol. 33, no. 3, pp. 1569–1574, 2017, doi: 10.13005/ojc/330363.

[41] Patiha, M. Firdaus, F. Rahmawati, S. Wahyuningsih, and T. Kusumaningsih, "Freundlich adsorption isotherm in the perspective of chemical kinetics (II); rate law approach," in *AIP Conference Proceedings [020037]*, 2020, vol. 2237, no. 020037, doi: 10.1063/5.0005342.

[42] T. Saka, L. San-Pedro, A. M. Abubakar, T. Sylvain, A. Budianto, and D. Houndedjihou, "Evaluation of the physical properties of various biomass materials for the production of activated carbon," *J. Chem. Environ.*, vol. 1, no. 2, pp. 30–39, 2023, doi: 10.56946/jce.v1i02.132.

[43] C.-F. Chang, C.-Y. Chang, and W.-T. Tsai, "Effects of burn-off and activation temperature on preparation of activated carbon from corn cob agrowaste by CO2 and steam," *J. Colloid Interface Sci.*, vol. 232, no. 1, pp. 45–49, 2000, doi: 10.1006/jcis.2000.7171.

[44] M. Kwiatkowski and T. Kopac, "An analysis of burn-off impact on the microporous of activated carbons formation," *IOP Conf. Ser. J. Phys. Conf. Ser. [ICMSQUARE 2017]*, vol. 936, no. 012090, pp. 1–6, 2017, doi: 10.1088/1742-6596/936/1/012090.

[45] M. Abdulrahim, S. Kiman, A. S. Grema, B. Gutti, and A. M. Abubakar, "An overview on the development of activated carbon from agricultural waste materials," *J. Eng. Manag. Inf. Technol.*, vol. 1, no. 4, pp. 207–211, 2023, doi: 10.61552/JEMIT.2023.04.006.

[46] A. Fernandez-Perez and G. Marban, "Visible light spectroscopic analysis of methylene blue in water: The universal calibration curve." Instituto de Ciencia y Tecnologia del Carbono (INCAR-CSIC), pp. 1–17, 2022, [Online]. Available: https://digital.csic.es/bitstream/10261/305439/1/Visible%2520light%2520spectroscopic_Fernandez_2022.pdf.

[47] SEE605A, "Introduction to sustainable energy technologies (SEE605A)-Experiment on photocatalytic degradation of methylene blue dye under visible light," Kanpur, Uttar Pradesh, India, 2023. [Online]. Available: https://home.iitk.ac.in/~ksnalwa/documents/Water Remediation- Lab Manual.

[48] F. Gritti and G. Guiochon, "Effect of the flow rate on the measurement of adsorption data by dynamic frontal analysis," *J. Chromatogr. A*, vol. 1069, no. 1, pp. 31–42, 2005, doi: 10.1016/j.chroma.2004.08.129.

[49] M.-R. Huang, H.-J. Lu, W.-D. Song, and X.-G. Li, "Dynamic reversible adsorption and desorption of lead ions through a packed column of poly (m-phenylenediamine) spheroids," *Soft Mater.*, vol. 8, no. 2, pp. 149–163, 2010, doi: 10.1080/15394451003756316.

[50] J. L. Knopp, K. Bishop, T. Lerios, and J. G. Chase, "Capacity of infusion lines for insulin adsorption: Effect of flow rate on total adsorption," *J. Diabetes Sci. Technol.*, vol. 15, no. 1, pp. 109–120, 2019, doi: 10.1177/1932296819876924.

[51] D. S. Perwitasari, Y. A. Y. Pracesa, M. A. Pangestu, and P. S. Tola, "Langmuir and Freundlich isotherm approximation on adsorption mechanism of chrome waste by using tofu dregs," in *2nd International Conference Eco-Innovation in Science, Engineering and Technology. NST Proceedings [2nd ICESET 2021]*, 2021, pp. 106–112, doi: 10.11594/nstp.2021.1417.

[52] V. Kutarov and E. Schieferstein, "Van der Waals equation for the description of monolayer formation on arbitrary surfaces," *Colloids and Interfaces*, vol. 4, no. 1, pp. 1–10, 2020, doi: 10.3390/colloids4010001.